Characterization and Evaluation of Nanofiber Materials

15

Taha Roodbar Shojaei, Abdollah Hajalilou, Meisam Tabatabaei, Hossein Mobli, and Mortaza Aghbashlo

Contents

Abstract

Characterization of nanofiber is performed to correlate test metrics with the practical characteristics of the material and to ensure reliable high quality of the products during production. The aim of single-fiber measurement procedure is to

T. Roodbar Shojaei (✉) · H. Mobli · M. Aghbashlo
Department of Mechanical Engineering of Agricultural Machinery, Faculty of Agricultural Engineering and Technology, College of Agriculture and Natural Resources, University of Tehran, Karaj, Iran

A. Hajalilou
Faculty of Mechanical Engineering, Department of Materials, University of Tabriz, Tabriz, Iran

M. Tabatabaei
Microbial Biotechnology Department, Agricultural Biotechnology Research Institute of Iran (ABRII), Agricultural Research, Education, and Extension Organization (AREEO), Karaj, Iran

A. Barhoum et al. (eds.), *Handbook of Nanofibers*,
https://doi.org/10.1007/978-3-319-53655-2_15

find fundamental information to better understand the relationship between the structure and the features of nanofibers. Theoretically, several characterization techniques have been utilized with nanofibers. Nevertheless, it must be borne in mind that morphology, molecular structure and mechanical properties are the most critical features of nanofibers. Therefore, in this chapter, it is attempted to explain briefly the nanofiber characterization techniques by focusing on the morphological and mechanical properties of nanofibers to provide fundamental data for evaluation of nanofiber materials.

Keywords
Nanofibers · Characterization · Polymers · Synthesis · Nanostructures

Introduction

There are great promises toward nanotechnology as a frontier research subject to boost sciences and strength industrial competitiveness. Nanotechnology is recently subjected to the remarkable governmental global investments at about 100 billion US dollars. The European Union has invested € 3.5 billion just for transnational cooperative projects on nanotechnology-related area. Recently, several fields of study and systems are matured by using nanotechnology and are progressively swamping markets and industries. Although, some issues and limitations such as a need for large-scale fabrication platforms, low chemical and biological flexibility, and economical and environmental challenges, i.e., toxicity aspects of nanomaterials, are still required to be addressed to fully understand the vast potential of nanotechnologies. Case in point, nanofibers could be considered as a relatively new developed type of nanomaterials, which can satisfy many of these abovementioned challenges. Advances in the supramolecular chemistry concept have introduced several self-assembled supramolecular polymers such as self-assembled monolayers, liquid crystals, and colloids. These theoretical and technical developments have enhanced the opportunity of using self-assembled molecules to generate nanofibers. Nanofibers can self-assemble from several ingredients, including polysaccharides and natural and synthetic polymers. In accordance with the physicochemical features of composed ingredients, two synthesis techniques are frequently applied to produce nanofibers: electrospinning and hydrogel formation. These methods are almost exceptional in being effectively large scaled in perspective. In addition, a variety of organic and inorganic materials can be used to synthesis and dope and modify the surface of nanofibers. For example, inorganic nanoparticles, carbon nanotubes, graphenes, photocurable compounds, low-molar-mass light-emitting molecules, biomacromolecules, cell-directing proteins, and growth factors have been used to functionalize nanofibers in order to increase their biocompatibility. Therefore, nanofibers are not only fascinating from a scientific perspective but also their fabrication procedures showing an outstanding potential to draw laboratory processes to the industrial scale. For these reasons, nanofibers could open up a new horizon for wide industrial applications of organic-based nanotechnology.

Background of Nanofibers

Nanofibers are described as nano-objects with two nano-sized external dimensions. It is defined as solid fibers with less than 100 nm in diameter and larger fiber length than that of the fiber diameter. Theoretically, the fiber length could be infinitely long. Therefore, the fiber diameter and length are the main external characteristics of fibers. Nanofiber's diameter is dependent on the used polymer type and the method of production ranging from a few nanometers to micrometers [28]. Nanorods, nanotubes, and nanowires are classified as rigid, hollow, and electrically conductive nanofibers, respectively. There are several types of nanofibers available, but the primary nanofibers of interest in the field of nanotechnology are formed from polymer precursors.

In the polymer nanofibers, the observed internal length is attributed to the fibers' molecular weight, which is defined as the persistence length or molecular length. The molecular length is the length in which the orientation of one part of a long molecule is corresponded to the orientation of another. As a result, the persistence length determines the stiffness of the molecule. Thus, the larger persistence lengths lead to the stiffer molecules. For instance, DNA shows the persistence length at about 50 nm, while the persistence length of a rigid rod could be infinite. In the weak molecules, the orientation of the end of the molecule shows low cohesion with the orientation of the inception of the molecule. The stiffness of the fiber is typically measured by the assortments and configurations of the molecules which form fibers, an entropic stiffness, not by the molecular stiffness.

Generally, nanofibers' stiffness would exceed the stiffness of the conventional-sized fibers. Mechanical properties of an individual nanofiber could be improved in comparison with their bulk or film materials counterpart. This improvement in mechanical properties is mainly contributed to the enhancement of the eventual alignment of polymer backbones along the nanofiber length as well as increase in the strength of filament-shaped materials as the fiber diameters decrease. The orientation of the molecular chains along the longitudinal axis would enhance the uniaxial tensile strength. The created fractures and cracks on the surface of nanofibers would weak the fiber's structure and facilitate their mechanical failures [29]. Fibers with smaller radius show lower external surface per unit length than that of larger radius fibers. Therefore, they would exhibit lower mechanical failure and surface cracks and flaws.

In addition, large surface to volume ratio of the nanofibers makes them an ideal alternative for conventional fibers. This feature improves their functionalizations, which give rise to obtain better flexible and strengthened materials. Consequently, it broadens the nanofiber utilizations in specific applications, e.g., as a component of larger structures such as nanomats and polymer scaffolds.

Porosity is another important property of nanofibers, which affects nanomaterial characteristics such as their fluid diffusion, wettability, controllable releasing of chemicals, and effective biochemical signal exchanging. Porosity can be a bulk property, an internal property, or a surface property of a sample. It is frequently defined as three-dimensional (3D), unfilled holes existed between nanofiber

ingredients and limited by fiber molecule bodies. The holes are connected hydraulically, which lead to continuous vessels available for fluids and molecules to flow through nanofibers.

Another unique feature of nanofibers is their promising optical property. The weak non-covalent intermolecular interaction leads to the small overlap between orbitals of different molecules and subsequently to strong optoelectronic properties in individual molecules. Generally, Frenkel excitons accurately describe initial excitations in the polymers. The Frenkel excitons are placed on individual polymeric chains with a considerable binding energy [67]. Excitation of the organic composite stimulated by an absorbed photon leads to an electronic transition from the highest occupied molecular orbital (HOMO) to the lowest unoccupied molecular orbital (LUMO) level. Although, the proximity between molecules in the nanofibers results in the generation of other excited species in which electrons are possibly transferred from one molecule to another close molecule. The most often-investigated energy transfer mechanism between two molecules is called fluorescence resonance energy transfer (FRET). In the FRET, the energy is transferred from an excited donor to an acceptor molecule through dipole–dipole interaction [76–78]. Since discovery of electroluminescence poly (p-phenylene vinylene) (PPV), organic, highly flexible optoelectronic materials have been advanced critically. Case in point, 1D nanostructures such as nanofibers, by presenting unique properties including processability, spectral tenability and chemical and biological compatibility have been considered as strategic nanomaterials for developing the next generation of optoelectronic devices based on organic semiconductors.

Due to the presence of bandgap energy of conjugated materials, nanofibers are considered as intrinsic semiconductor materials [2, 10]. Conductivity property of conjugated materials was first observed in 1976 in doped polyacetylene [29, 67]. The conductivity of polymer nanofibers can be enhanced by doping, while un-doped nanofibers have also shown strong conductivity. Nanofibers by presenting high conductivity have attracted a great deal of attention and opened up a novel field of study at the frontier of chemistry, physics, materials sciences, and nanotechnology [16, 29]. This characteristic in the conjugated materials is largely attributed not only to properties of individual molecules but also to the supermolecular assembly of the molecules. Indeed, the electrical conductivity is due to the charge-carrier transport by band-like conduction or by hopping mechanism [35]. For example, due to the overlap between adjacent carbon orbitals along molecular backbones, charge carriers are delocalized along the conjugation length. Thus, the mobility along the intramolecular length becomes high [23, 29]. The presence of material disorders, chemical defects, and the molecular distortions could limit the transport of charge carriers fundamentally. Generally, nanofiber molecules are assembled with π-π interaction, which provides an intermolecular mobility [22, 57, 93, 97]. Most of light-emitting nanofibers also show conductivity because of their conjugation characteristics. It is possible to fabricate several other conductive nanofibers by using different synthesis techniques [51, 102]. It has been proven that nanofibers are considerably attractive for investigation of charge transport theories at nano-sized scale due to their unique behaviors, i.e., possessing smaller particle size, large surface to volume ratio, chemical flexibility, and controllable molecular configuration [89].

Synthesis Process of Nanofibers

The most frequently used technique for the synthesis of nanofibers is electrospinning. This process was first developed by Formhals in the 1930s decade to produce fibers. In this technique, a solution is charged by using a high-voltage electric field (10–50 kV) to produce charge carriers with the same polarity as the used electric field. Due to the presence of analogous charges, the electrostatic repulsion tensions the solution forward in a cone-like form. When high-voltage electric field is applied, the fiber jet formation is occurred at the cone tip, and the opposite charged collector collects the formed nanofibers [88] (Fig. 1). Although electrospun nanofibers have been used in several applications including tissue engineering, filtration, organ implant, gene and drug delivery, diagnosis, optical platforms, and wound dressing, there are still definite limitations and requirements on the production of nanofibers by using electrospinning. With this regard, hydrogel formation as an alternative technique is introduced to produce nanofibers from oligomeric biopolymers [25, 83]. Hydrogelation is an obvious macroscopic shift in texture and morphology of materials which provides visual information on successful formation of nanofiber self-assembly.

Nanofibers can be synthesized from natural polymers such as keratin, collagen, silk, alginate, gelatin, chitosan, and celluloses as well as synthetic polymers like poly lactic acid (PLA), poly lactic-co-glycolic acid (PLGA), poly caprolactone (PCL), and polyurethane (PU). The polymer chains are spun into the fibers through covalent bonds by using different organic solvents such as ethanol, chloroform, formic acid, and water. Diameter and surface topology of the nanofibers are strongly dependent upon the surface free energy, surface tension, solution concentration, solvent permeability, electrical conductivity, polarity, and viscosity. In

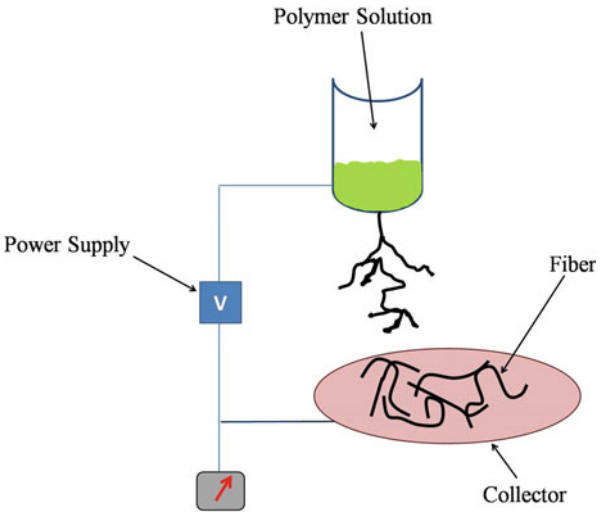

Fig. 1 Schematic representation of the electrospinning process to produce nanofibers

addition, the physical parameters of the processing equipment as well as ambient factors of the procedure could also modulate nanofiber generation [37].

Nanofibers could easily degrade under harsh reaction conditions such as exposure to gamma radiation, plasma, high-temperature ultraviolet, and acidic or basic environments. Therefore, when degradable polymers are used in sensitive applications, particular care should be taken to preserve nanofibers from rapid destruction or degradation. In order to obtain this, surface modification of fibers by coating or layering as well as functionalizing of nanofibers are widely used. In fact, this process is carried out by using electrostatic interactions to immobilize biomolecules on the surface of nanofibers [62].

Characterization of Nanofibers

Characterization of nanofibers is correlating test metrics with the practical characteristics of materials and verifying the quality of products during the synthesis procedure. By single-fiber characterization, fundamental data are obtained to understand the relationship between the structure and the properties of nanofibers. Theoretically, several characterization techniques can be utilized for nanofibers. In addition, entire available polymer characterization techniques can be used for organic polymer nanofibers.

A principal limitation in characterization of nanofibers is the lack of confirmed appropriate techniques. There are some challenges in the characterization of nanofiber, including limitation in the manipulating small nanofibers, finding an appropriate observation mode, finding a suitable source for force transducers and actuators, and single nanofiber sample preparation [86]. It seems that, nowadays, some of these limitations are not that serious anymore and have been improved. For example, high-resolution nano manipulators and single-fiber isolation by using simple sample preparation procedures have solved some of the abovementioned limitations.

The type of characterization approach used for testing nanofibers is based on the ultimate ambition of as-prepared materials. For instance, when nanofibers are intended to be used for air filtration in gas masks, the air permeability, particle penetration, porosity distribution, and residual electrical charge on fibers are important. If it is going to be used for sensors, the electrical conductivity, optical characteristics, equilibrium swelling by organic vapors, and chemical reactivity may be meaningful to be tested.

Evidently, the characterization techniques are still in initial stage and the demand for the establishment of an efficient characterization techniques are increasing continuously. Therefore, in this section basic information for the selected characterization methodologies, which are used for nanofibers, are reviewed in summary. Some of these methodologies are adopted as standard test methods in the field from the American Society for Testing and Materials (ASTM) or the International Organization for Standardization (ISO). It is also attempted to provide some information on the limited single-fiber assessment techniques.

Morphological Characterization of Nanofibers

Pore Size Distribution and Porosity

As explained before, porosity is a morphological property which is defined as empty voids existed between nanofiber ingredients. The pore size distribution and porosity are the important characteristics for scaffold and filtration. According to the standard guide and literature review, porous materials are classified based on their pore sizes as presented in the Table 1 [90].

There are three different types of pores including through pores, blind pores, and closed pores as shown in Fig. 2.

Several techniques are available for characterization of porous materials including mercury intrusion porosimetry, liquid extrusion porosimetry, nuclear magnetic resonance, and capillary flow porometry.

Mercury Intrusion Porosimetry

Mercury intrusion porosimetry is the conventionally used technique for the porosity assessment, in which mercury is forced into the nanofiber sample by using a pressure "p" to the mercury column. By increasing "p," smaller voids in the nanofibers are intruded by the mercury. This technique just measures the voids that are accessible by the mercury. It simply means that the small or closed pores, that are inaccessible, are not involved. The large voids are also not considered in the measurement process since the mercury floods easily even before the pressure application. Washburn

Table 1 Classification of pores based on pore sizes in the porous materials

Title	Size (nm)
Micropores	0.5–2
Mesopores	2–50
Macropores	50–200
Capillaries	200–800
Macrocapillaries	>800

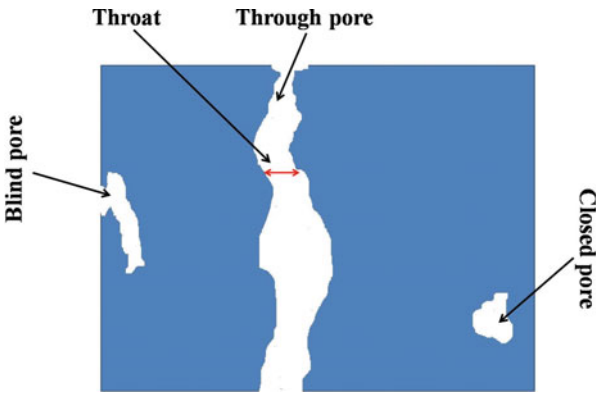

Fig. 2 Different types of pores in a porous material

equation (Eq. 1) measures the relationship between the used pressure "p" and the pore radius "r" as follows [45]:

$$r = -2\gamma \cos\ \theta/p \tag{1}$$

where γ and θ are the contact angle and the surface tension of the mercury, respectively.

Since in the mercury intrusion test more than thousands of psi pressure is used, the pore volume distribution, pore size, and pore shape could be distorted in those nanofibers that are made of soft polymers. By using this technique, the voids from both sides of the sample are determined. The porosity of poly (lactide-co-glycolide) (PLGA) electrospun from THF/DMF mixed solution was measured at 91.6% with pore volume of 9.69 mL/g and pore sizes of 2–465 mm [56]. In another study, Poly (L, lactide) (PLLA) showed 78% porosity with mean pore diameter of 21.5 mm [94].

Liquid Extrusion Porosimetry

Since in the mercury intrusion porosimetry high pressure is applied, it is not applicable for the soft polymeric nanofiber identification. Therefore, liquid extrusion porosimetry was developed to measure porosity of nanofibers, where lower orders of pressure are applied compared to the mercury intrusion porosimetry technique. In liquid extrusion porosimetry, a nanofiber is placed on a porous membrane, and it is covered by a wetting liquid layer. The liquid is then intruded to the voids by gas pressure over the liquid column. The liquid is then transferred from the pores of porous membrane to the fiber. The pressure and volume of liquid are recorded. The pressure "p" and the volume of liquid are indicative of the pore diameter and pore volume, respectively. The relationship between pressure "p" and the average pore radius "r" is measured by the following equation (Eq. 2)

$$r = 2\gamma \cos\ \theta/p \tag{2}$$

where γ is the contact angle and θ is the surface tension of the liquid.

"V," volume of liquid, is attributed to the shift in the interfacial area at interface of the liquid/polymer as given below [42]:

$$pdV = \gamma \cos\theta dS \tag{3}$$

where "*S*" is the surface area and measured by integration of the function.

Any pores that are not accessible by the liquid cannot be investigated by this technique. Their fractions can be indirectly assessed by comparing liquid extrusion records to the intrusion porosimetric information. This technique also measures the required pressure to intrude liquid to the pores. The pore volumes and the pore dimensions are measured by using liquid extrusion that are attributed to the gas flow direction.

The measured pore size distributions by using both mercury intrusion and liquid extrusion methods are generally different. The liquid extrusion porosimetry technique is mostly underestimate the pore volumes for pores with large surface

openings in related to those assessed by mercury intrusion porosimetry. The channels' pore volume is measured based on the throat diameter.

Capillary Flow Porometry

Capillary flow porometry technique is similar to the liquid extrusion, in which, nanofibers are saturated with a liquid under gas pressure. In this technique, gas pushes the liquid and the gas flow rate as a function of the differential pressure is monitored. The lower pressure at which the larger voids are wiped and gas is flowed through the pores is known as bubble point. The gas pressure would not make any distortion in fiber's pore structure. The required flow rate is significantly dependent on the liquid's surface tension, fibers' surface energy, and diameter of pores.

Nuclear Magnetic Resonance

Nuclear magnetic resonance (NMR) is infrequently used to characterize nanofiber porosity. This technique relies on the differences between t_1 and t_2 proton relaxation times in liquids. The difference between t_1 and t_2 will decrease with the increase in average pore diameter. In the NMR, in magnetic field nuclei absorb and reemit an electromagnetic radiation. This radiation has precise energy at a specific resonance frequency, which is dependent on the potency of magnetic field as well as the magnetic characteristics of the atoms' isotope. By using NMR, observation of the nucleus' exact quantum mechanical-magnetic features is possible. The resonance frequency of a particular material is corresponded to the strength of the used magnetic field.

For example, the porosity of poly (3-hydroxybutyrate-3-hydroxyvalerate) (PHBV) films was studied by using NMR. It was observed an increase in the differences between t_1 and t_2 by increasing in the immersion time [63]. In another effort, the porosity of polycaprolactone (PCL) was estimated by using NMR at 78 + 3%. No significant differences were found in the average porosity related to the average fiber diameter [6]. The structures of the polymer molecules within the nanofibers can also be characterized by NMR analysis.

Microscopic characterizations are frequently applied as the preliminary characterization techniques. Both optical and electron microscopy have been routinely used to monitor diameter distributions of nanofibers. Since most of the pores are not cylindrical with regular geometry, using optical and electron microscopy determines only the surface of voids, and the porosity data obtained are different from those that are measured by other methods.

Diameter and Size Distribution of Nanofibers

Transmission Electron Microscopy (TEM)

The transmission electron microscope opened up a new window to visualize the structure and morphology of materials far below the resolution presented in light microscopy. TEM is considered as one of the most important instrument for many aspects of different fields of study.

TEM is a destructive technique, in which, the sample may be damaged by the electron beam, especially when biological samples are analyzed. The regular imaging process commences by transmitting a beam of electrons through the ultrathin section of samples which leads to a phase shift in a portion of the electrons. When the incident electron beam comes down through the microscope column, it interacts with the sample fluorescent screen. During the hitting of the electron beam to the sample, a large amount of radiation is transmitted/emitted from the sample.

Interaction of the electron beam with the nanofibers leads to the elastic and inelastic scattering of the transmitted electrons. The images are visualized from the elastically scattered electrons, allowing observation of the structural features or defects at a high resolution. The elastically scattered electrons can also be used in the diffraction mode to provide crystalline structure data.

Scanning Electron Microscopy (SEM)

In scanning electron microscopy, surface of the samples is sputtered with a thin layer of gold and is placed in high-energy electron beam under vacuum. A cathode source as an electron gun generates beam and collimates by electromagnetic lenses to an adjusted spot. The spot is manipulated by several deflection coils and surface of the samples is scanned. Interaction of the beam with the secondary electrons produced from the samples is monitored and amplified by using scintillator and photomultiplier tube, respectively, and illustrated in the form of a high-resolution image of the sample surface. Interactions of the beam with some of the secondary electrons produced from the samples emitted at near 1080 can form some backscattered electrons which are attributed to the atomic number of the scattering surface. Since, the SEM is mostly unapplicable for the nano-sized materials, a field emission electron microscopy (FeSEM) is employed for observation the morphological behavior of the samples at relatively high resolutions.

Both FeSEM and TEM have been extensively used in understanding and quantifying of the morphology of nanofiber. Moreover, FeSEM and TEM can provide three-dimensional (3D) and two-dimensional (2D) images for void and nanofiber morphology with 1–20 nm and 0.1 nm resolutions, respectively.

FeSEM gives topographic information from the surface or whole small particles. It uses electrons instead of light which is released from a field emission source and accelerated in a high electrical field gradient. These liberated electrons are focused onto the sample (primary electrons), and as a result, the electrons are reflected and directed back from sample (secondary electrons). The surface structure of sample would change the angle and velocity of these secondary electrons and catch via a detector. This technique is mostly equipped with the energy dispersive X-ray (EDX) spectroscopy to obtain information related to the elemental features or compositions. Indeed, an X-ray excited from the interaction of electron and sample is used to identify the elemental and chemical composition of the sample. To maximize the X-ray signal reaching the detector, the EDX spectrometer is often located close to the sample. An EDX spectrum is consisted of peaks of modifying energy. Since X-rays include certain energies that are respective to each element (like fingerprinting), the peaks in the EDX spectrum are performed to determine the elements within a sample.

Observation and assessment of nanofibers, biological material, live cells, or even living organisms by using environmental SEM (ESEM) without any sputtering and coating treatment requirement are also possible. In the ESEM, the electron beam is manipulated under water vapor environment. In this case, the accumulation of surface charges is prevented by ionization of water, allowing non-conductive materials to be accurately visualized without sputtering requirement. The ESEM could be supplied with the EDX as well.

In several studies, FeSEM or SEM has been used to characterize different nanofibers by monitoring 60 [66], 100 [30, 47], and 500 [71] measurements per micrograph averagely to determine nanofiber diameter. In another studies, the morphological structure and nanofiber diameter for PVA [79], kefiran nanofibers [24], polyamide 66 (PA66) [32], poly (vinyl alcohol) (PVA) [52], poly (lactic acid) (PLA), poly(ethylene oxide) (PEO), poly(ε-caprolactone) (PCL) [69], poly (vinyl pyrrolidone) (PVP) [44], and modified cellulose/poly (vinyl alcohol) (MC/PVA) [12] were monitored via these techniques.

Since images recorded by using microscopic techniques are limited to a random small section of the sample, the data obtained cannot be considered as a general characteristic of the entire sample. Case in point, for nanofiber qualitative characteristics, an adequate number of random samples are required to be selected to obtain sufficient statistical information and accurate characteristics of the materials.

Determining fiber diameters by automated analysis of the images using image analysis tools is used widely. For example, Fovea Pro (Reindeer Graphics Inc.) and ImageJ software (National Institute of Health, USA) as image analysis tools are used to determine distribution of fiber diameters. In these cases, a sufficient number of images and fibers per images are required to estimate the fiber diameter.

Atomic Force Microscopy (AFM)

Atomic force microscopy is considered as an extensively used technique for the characterization of nanomaterials. It gives information about topography, morphology, and particle/grain distribution from the surface of the sample. In AFM, a 15-μm-long monolithic silicon-made tip or a probe located at the end of cantilever is pressed against the sample with an invariable force to scan the surface of the samples. The probe movement is converted into the signals to depict sample surface. Its movement, as small as 1 nm, can be probed by instrument. Reflection of the laser beam off the surface of the cantilever is generated because of the variations in tip-to-surface distance that is monitored by a position-sensitive photodiode detector (Fig. 3).

The interaction loop between the photodiode regulation and the piezoelectric scanners to the tip movement would provide data, which are used for image generation. Therefore, in AFM a minute deflection can even be detected by the photodiode detector. In the contact mode imaging, the tip is vibrated at a low frequency where it touches the surface of sample alternatively. Imaging can be carried out with the oscillating cantilever in which the tip is not in contact with the surface, but in close proximity above the surface of sample. In this mode, the frequency and amplitude of the oscillating cantilever are recorded to generate an image [7]. In summary, normally, the operation of AFM can be carried out by two

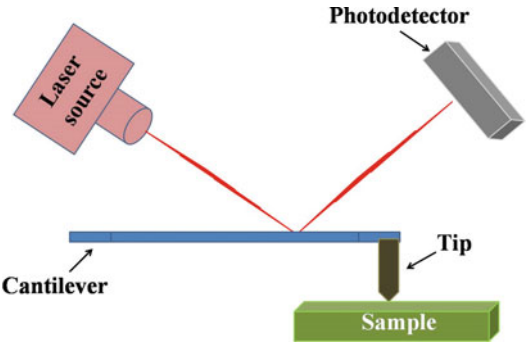

Fig. 3 Atomic force microscope sample characterization

modes depending on the application: non-contact and contact modes. The silicon or silicon nitride cantilever with the sharp tip (radius in nano-sized scale) at its end scans the surface of the bulk samples and gives information by taking picture.

The topology of several nanofibers including polyurethanes, aramids, poly (dicyclopentadiene), poly (butylene terephthalate) (PBT), polyelectrolyte complexes, silk nanofibers, polyacrylonitrile (PAN), polystyrene (PS), poly (benzimidazole), PEO nanofibers, and polylactide (PLA) has been investigated through AFM images [4, 18, 20, 36, 43, 49, 64, 68, 84, 86, 94].

Characterization of nanofibers by AFM is normally a complicated procedure, and due to the convolution of the shape of the tip with the nanofiber geometry, the width of fibers obtained by AFM is not accurate [49]. The exaggeration of the fiber diameter measured by AFM was confirmed when fiber diameters of poly (benzimidazole) (PBI) nanofibers were twice larger than that of measured by other techniques. Generally, the fibers with the smaller dimension present a higher exaggeration in AFM [68]. Mostly, the resolution of AFM images can be poor even when a sharp tip is used and the nanofibers tend to be easily displaced by the movement of the tip over their surface. In order to solve these problems, nanofibers are placed on a substrate to fix them during measurement via adhesion or nonbonded interactions.

Mechanical Characterization of the Nanofibers

The characterization techniques used to assess the mechanical properties of films and textile materials can be utilized with some modification to nanofibers. In this case, the data interpretation should be done cautiously. One of the most frequent techniques used to determine the mechanical properties of nanofibers is tensile test by applying the same general experimental procedure used for film or woven textile samples.

Tensile Test

In order to test nanofibers by using tensile test, the samples are cut into the rectangular or typical dumbbell-shaped test samples [9, 21, 54, 61, 72, 100]. The universal testing machine is applied to determine the tensile properties of nanofibers.

For instance, the mechanical properties of 100-mm-thick poly (vinyl alcohol) (PVA) nanofiber were tested by using a 1 cm length gauge with 2 mm/min crosshead speed [92].

In the tensile test process, the sample is placed in the universal testing machine and extended slowly until it fractures. The gauge elongation is recorded against the applied force. The data obtained do not define the geometry of the sample surface so it needs to be manipulated. The elongation records are used to calculate the engineering strain, ε, as follows:

$$\varepsilon = \frac{\Delta L}{L_0} = \frac{L - L_0}{L_0} \tag{4}$$

where ΔL, L_0, and L are the change in gauge length, initial gauge length, and the final length of gauge, respectively.

The force data are used to calculate the engineering stress, σ, as follows:

$$\sigma = \frac{F_n}{A} \tag{5}$$

where F and A are the tensile force and the nominal cross-section of the sample, respectively.

Since the mechanical impeccability and the geometric arrangement of the fibers can be compromised during sample preparation, handling fragile nanofibers is still a critical concern. Instead of thickness an equivalent thickness can be predicted from the "ρ," density of polymer, mass m, and "A," the die area utilized for cutting the samples [65]:

$$\text{Equivalent thickness} = m/A.\rho \tag{6}$$

The mechanical properties of nanofibers are affected by the chemical-unassociated factors of the polymers. Nanofibers of the same polymer electrospun produced from different solvents often show diverse mechanical properties. These discrepancies are related to the diverse rates of solvent evaporation and subsequently different kinetics of development of the relevant phase morphologies which affect nanofiber morphology. The tensile properties of a sample are affected by several factors, including the volume density of fibers, fusion degree of the individual nanofibers, the multi-dispersity of fiber diameters, and deficiency and branching of fibers even when the same polymer/solvent materials are used. For example, pellethene nanofibers electrospun from THF and DMF provide diverse tensile properties [80].

Dynamic Mechanical Analysis (DMA)

By using dynamic mechanical analysis (DMA), the viscoelastic features of the samples are determined. In this test, the fiber and film clamps are used for the oriented and unoriented samples, respectively. A DMA multifrequency strain process is generally run with a temperature and frequency uniform changes to test a

cylindrical sample with length "l" and diameter "d." The master curves are plotted based on time versus temperature, when the middle of the experimental temperature, reference temperature, is selected and the other curves are changed regarding the reference curve. Several properties for the trends such as loss modulus, storage modulus, and tan δ master curves could be tested as a function of nanotube loading. Moreover, the Arrhenius equation is used for the calculation of the nanofibers' activation energy as below (Eq. 7):

$$\ln a_T = \frac{-E_a}{R}\left(\frac{1}{T_0} - \frac{1}{T}\right) \tag{7}$$

where E_a, a_T, R, T, and T_0 are the activation energy of the fibers, time-based shift factor, gas constant, temperature in which measurement is performed, and the reference temperature, respectively.

The master curve is obtained by horizontally shifting the curves around a reference temperature. The time-based shift factor, a_T, for each temperature is plotted as a function of the temperature. When the polymer is strained, the energy barrier should be beaten to allow chains to shift or spin around the main chain bonds. This energy barrier is defined as the polymers' activation energy. The activation energy is increased to the maximum with addition of the nanotubes, same as the effect of nanotubes on the tensile properties of materials. By adding high modulus nanotubes, the resistance to strain, rupture, and deformation is increased significantly. Although, by increasing the concentration of nanotubes, the reinforcing effect is decreased.

Structural Evaluation and Phase Formation Study

X-Ray Diffraction (XRD) Technique

X-ray diffraction spectroscopy is a type of nondestructive test which can be conducted on both powder and pellet form samples. It is mostly applied to investigate the structural and phase evaluation of materials. In fact, it gives information about the phase formation, crystallite size, lattice strain, lattice parameter, d-spacing, and content of each phase. The sample preparation was carried out by sticking a double-side adhesive tape in the dimension of 1*1 Cm^2 on a piece of glass plate. Then, the as-enough powders are dispersed on the surface of the tape so that it is completely covered. The XRD spectra are collected applying, e.g., a Philips X'Pert-MPD machine equipped with a graphite monochromator. Depending on the type of tool, the applied current and voltage would be ~30 mA and ~40 kV, respectively, and Cu Kα radiation ($\lambda = 0.1542$ nm) performing scan rate of 0.030 2θ/s. Figure 4 displays a schematic diagram of how a quality data is collected without intricate sample preparation.

A small portion of the powder is placed in a sample holder to radiate with X-ray of a fixed wavelength. A goniometer is used to record the intensity of the reflected radiation. This information is then evaluated for the reflection angle to estimate the inner atomic spacing (D). The intensity (I) is evaluated to distinguish (applying I

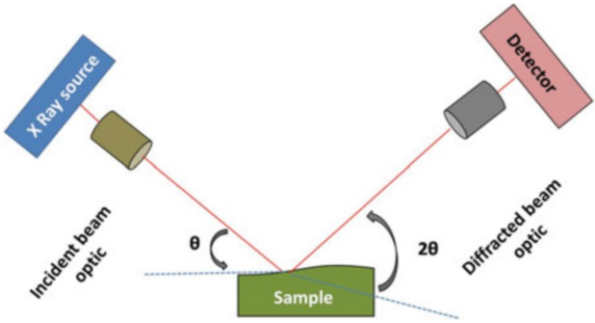

Fig. 4 Schematic diagram of the XRD

ratio) the different D spacing, and the results are to determine possible matches. A simple version of Bragg's Law for powder diffraction is exhibited in Eq. 8 [27]:

$$n\lambda = 2d \sin\theta \tag{8}$$

where θ, d, λ, and n designate the Bragg angle (Fig. 4), distance between atomic layer, the electron beam wavelength, and an integer, respectively. Sets of atomic planes within a crystal structure resulted in constructive diffraction if the incident beams strike them at the Bragg angle (θ). Atomic planes, (h k l), from which d_{hkl} values are identified, are indexed applying conventional Miller index notation. The average crystallite size was calculated from different methods to ensure the accuracy of their size. Firstly, to determine crystallite size, the Debye-Scherrer's equation was exploited using the Eq. 9 [33]:

$$d_{(h\ k\ l)} = \frac{k\lambda}{\beta \cos\theta} \tag{9}$$

where, λ, θ, and β designate wavelength radiation ($\lambda = 0.154$ nm), Bragg diffraction angle, and full width of the diffraction line at half the maximum intensity (FWHM), respectively. K is a constant, usually taken to be equal to 0.9 [33].

FWHM designated by β depicts peak broadening which can be related to the discrepancy in integral profile width between a measured FWHM (βi) and equipment broadening (βe); therefore, a refined version of β was used based on the following equation in order to remove the errors due to the instruments [70].

$$\beta^2 = \beta i^2 - \beta e^2 \tag{10}$$

Prior to estimating the crystallite size and lattice strain from XRD peaks and in order to refine the data, the background was automatically eliminated, and the exact position of $k\alpha 1$ and $k\alpha 2$ radiations was analyzed using the X'Pert High Score software:

$$\frac{k\alpha 2}{k\alpha 1} = 0.51 \tag{11}$$

X'Pert High Score software executes the pseudo-Voigt profile function, which is the weighted average between a Gaussian and a Lorentz function [70]:

$$G_{ik} = \gamma \frac{c_0^{1/2}}{H_k \pi} \left[1 + C_0 X_{ik}^2\right]^{-1} + (1-\gamma) \frac{c_1^{1/2}}{H_k \pi^{1/2}} \exp\left[C_1 X_{ik}^2\right] \quad (12)$$

where X_{ik} is considered as $(2\theta_i - 2\theta_k)/H_k$, herein, H_k is the β value of the K^{th} Bragg reflection, γ is a variable "mixing" parameter that yields the Lorentzian profile amount in terms of the Gaussian profile amount, and C_0 and C_1 are taken to be 4 and 4× ln 2, respectively. Thus, the overall profile shape is presented [33].

The level of crystallinity in several nanofibers including poly (D,L lactide) (PDLA), PLLA [99], PLGA [100, 101], poly (m-phenylene isophthalamide) (PMPI) [58], polyamide 66 (PA66) [32], poly (glycolide) (PGA), poly (vinyl alcohol) (PVA) [52], poly (ethylene oxide) (PEO) [69], poly (lactic acid) (PLA), poly (ε-caprolactone) (PCL) [69], PET, PEN [48], PAN [41], poly (vinyl pyrrolidone) (PVP) [44], and nylon-6 [19, 59] was assessed by XRD technique. The results showed a relatively low level of crystallinity for most of the studied nanofibers, while a relatively high level of molecular orientation was observed. Since electrospinning process is rapid and yielded metastable amorphous nanofibers, the development of crystallite during electrospinning process is retarded [8].

Chemical Characterization of Nanofibers

X-ray Photoelectron Spectroscopy (XPS)

Most surface characteristics, such as hydrorepellence, wettability, adsorption, and adhesion, of materials are strongly attributed to their microscopic properties, such as elemental and molecular composition, microporosity, and roughness. Knowledge of the surface dynamics of materials has recently allowed significant progress in many academic and scientific fields [91]. So far, many electron spectroscopy techniques have been developed as potential methods for surface analysis.

Among these tools, X-ray photoelectron spectroscopy (XPS) is considered as one of the most powerful techniques, which typically gives accurate chemical information about the surface of the materials, in the case of elemental and molecular composition. It is also a strong technique enough to distinguish chemical states of the same element in order to determine their depth distribution at a range of thickness of about 5–10 nm. Furthermore, detection of the emitted electrons through electron counter creates an opportunity to implement both the quantitative and qualitative analysis [81].

This technique is normally used in parallel with Auger process with a difference that it is a one-electron process and the photoelectron kinetic energy is dependent upon the excitation radiation energy. The photoelectron kinetic energy is obtained around 0–1400 eV when the most commonly excitation sources are employed. XPS is less likely to yield surface damage, and it can be preferable especially in non-conductive materials, studying the nature of surface. So far, however, several techniques have been employed to study the surface of treated materials; they,

sometimes, do not involve key aspects of natural and synthetic materials. For example, studying the functional groups induced onto nanofiber materials through the surface treatment is only possible to carry out via XPS. In other words, induced various functionalities during the surface treatment of nanofiber materials affect their properties, which is difficult to evaluate by means of other techniques. Therefore, understanding the surface features of such materials via XPS is very essential and inpriority.

XPS measurements are accomplished, e.g., with a ULVAC-PHI Quantera II system equipped with monochromatic Al-Kα (hv = 1486.6 eV) X-ray source. The experiments would operate at 25.6 W (beam diameter of 100 mm), wide scan analysis (pass energy of 280 eV with 1 eV per step), and narrow scan analysis (pass energy of 112 eV with 0.1 eV per step). The sample is pressed on the indium foil prior to place in the high vacuumed chamber. The binding energy (BE) of the XPS system is calibrated by setting C1's peak at 112 eV [35].

Surface physicochemical characteristics of surface-treated nanofibers are normally sensitive to preparation methods and chemical and/or physical routes, which makes remarkable variations in the surface of materials. For example, studying silver nanofiber/polyvinylpyrrolidone (AgNF/PVP) core–shell nanofibers through XPS, prepared via coaxial electrospinning process, indicated the presence of elemental composition on the surface of AgNF/PVP core–shell ES nanofiber mats with a desired composition [26]. From XPS spectrum, only peaks related to C, N, and O emerged in the spectrum. Surprisingly, the XPS results revealed the absence of silver on the AgNF/PVP core–shell ES nanofiber mats' surface. Due to the fact that elemental analysis of XPS can determine the topmost ~100 Å in depth of a tested sample [85], it is reasonable to draw a conclusion that the Ag signal in the PVP shell surface was at least deeper than 10 nm so it could not be observed. The above results indicate that the formed AgNF/PVP core–shell ES nanofiber mats are corresponding with the ideal nanofiber model.

In another study, chemical composition and structure of p-PAN/CNC/Ag nanofibers are investigated [74]. The XPS results are shown in Fig. 5. C, N, O, N, C, and Ag peaks were observed in the p-PAN/CNC/Ag nanofibers. Figure 5b shows a high-resolution XPS of Ag 3d. The p PAN/CNC/Ag nanomats represented two specific peaks. Their binding energy was about of 369.6 and 375.6 eV, which belongs to Ag $3d_{5/2}$ and Ag $3d_{3/2}$ energy levels, respectively. The spine energy separation is 6 eV, reflecting the metallic nature of Ag [14]. The N 1s levels (Fig. 5c) showed only one peak at 398 eV, which is attributed to nitrogen atoms present in nitrile structures (CN) [73]. The high-resolution XPS of O1s is shown in Fig. 5d. The –OH peak in the nanomat appeared at 532.0 eV. As compared to the previous works, it moved to lower values. The reason is associated with the O-electron cloud density reduction in –OH of the p-PAN/CNC/Ag system. This signifies that O chelated with silver ions [95]. The Ag ions were chelated between the hydroxyl sites of Ag ions and CNCs, but the cyano groups of PAN. CNCs in these electrospun nanostructures binding the PAN with the metallic nanostructure by H-bonds. This results in a good foundation for the metallic/CNC/PAN nanocomposite materials. Peaks located at 530.9 eV and 529.5 eV were attributed to C=O and Al_2O_3. These peaks are induced by the residual solvent and aluminum foil used to collect the fibers [95].

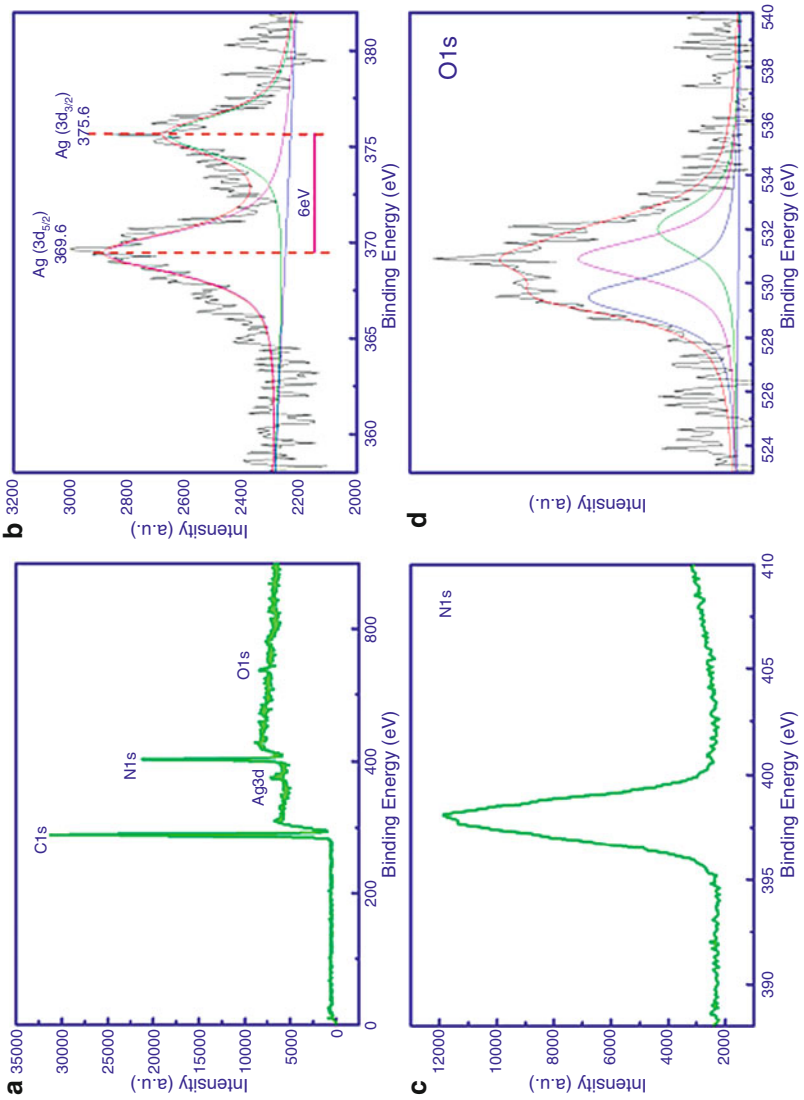

Fig. 5 XPS spectra of the P-PAN/CNC/Ag nanofibers (**a**) Ag 3d, (**b**) N 1s (**c**), and O 1s (**d**) [74]

Fourier Transform Infrared Spectroscopy (FT-IR)

The term Fourier transform infrared spectroscopy (FTIR) refers to a recent advance in the manner where the interference pattern data is collected and converted to a spectrum. Indeed, infrared radiation is passed through a sample and different phenomena occur. The emitted radiation could be absorbed, passed, and/or transmitted from the sample. The obtained spectrum provides some information about molecular transmission and absorption which yields molecular fingerprint for the materials.

The wavelength of absorbed light shows characteristic of the chemical bond, which is observed in spectrum. Similar to a human fingerprint, no two individual molecular structures generate the same infrared spectrum. This feature makes FTIR useful for a number of analyses such as identifying unknown materials, determining the quality of a sample, and determining the value of components in a mixture.

The functional groups of the several nanofibers such as poly (vinyl alcohol) (PVA) [52], modified cellulose/poly (vinyl alcohol) (MC/PVA) [12], polyamide 66 (PA66) [32], poly (lactic acid) (PLA), poly (ethylene oxide) (PEO), poly (ε-caprolactone) (PCL) [69], and poly (vinyl pyrrolidone) (PVP) [44] were investigated using FTIR spectroscopy. The strength of molecular interaction between polymers inside the nanofibers could be investigated by using FTIR as well [44].

Raman Spectroscopy

Raman spectroscopy is used to evaluate the rotational, vibrational, and other low-frequency modes in physical or chemical systems. It depends on inelastic scattering, or Raman scattering of monochromatic light in the near-infrared or near-ultraviolet and visible range, typically generated from a laser source. Indeed, the interaction of laser light with phonons or other excitations leads to the energy of the laser photons being moved up or down. The change in the laser photons' energy provides information about the phonon modes in the system.

Raman spectroscopy has been widely used for different nanofibers to investigate the considerable variations in the distribution of the polymers and to assess the presence of carbonaceous materials within the polymeric nanofiber matrix and their effects on the morphology and physical properties of the nanofibers [15].

Polystyrene nanofibers loaded with different amounts of MWCNTs were investigated by using Raman spectroscopy. The D and G bands of MWCNTs as the main Raman bands showed a significant increase in the intensity of bands because of MWCNT dispersion in polystyrene. The observed modification in Raman bands is attributed to the stress transfer from polystyrene to MWCNTs [15]. In another try, the D and G bands of the poly (acrylonitrile) (PAN)-based carbon nanofibers were studied to determine the crystallite sizes. The D and G bands, which are attributed to sp^2 carbon species, were fitted into a Gaussian–-Lorentzian hybridized function. The crystallite sizes of nanofibers were determined from the ratios of the intensity of the G to that of the D band [46]. Raman spectroscopy has also been utilized to study the effects of CNTs on composite nanofibers of silk, carbon fibers, and PAN.

Thermal Evaluation Techniques

In the thermal analysis, a physical behavior of a material is determined in terms of temperature, where a controlled temperature program is employed. Thermogravimetric analysis (TGA) is being used to dictate an occurred variation in weight of material (loss or gain) as a function of alter in heating temperature. Differential scanning calorimetry (DSC) comprises cooling or heating test and relies on differences in energy required to keep the sample and reference at an identical temperature. The temperature differences between an inert reference material and a sample is determined by using differential thermal analysis (DTA), when both are treated with the identical heat. The analysis of thermal feature of the materials is carried out by using DTA, thermogravimetric analysis (TGA), and differential scanning calorimetry (DSC).

Differential Scanning Calorimetry Technique

In the differential scanning calorimetry (DSC) techniques, a sample is sealed in aluminum or platinum crucible (sample pan), and a reference sample free aluminum pan is manipulated at the same temperature. The sample pan with higher thermal aptitude will request additional thermal energy attributed to the reference sample free aluminum pan to reach an applied temperature. When the insulated precincts' temperature raised, the change in the energy requirement for the both reference sample free aluminum pan and the sample could be monitored precisely. In the thermal behavior, several distinctive prototypes such as first- and second-order transitions, solution evaporation, and chemical reactions can be observed.

The sample and reference pans could be placed in an insulated chamber with an efficient thermal contact with each other through a metallic connector. The existence of nanofibers inside the pan will induce thermal imbalance followed by heat flow between sample and reference pans. The enthalpy changes can be measured by estimating the difference in temperature between the pans, ΔT. The nanofibers will encounter melting of the crystalline fraction, as an endothermic event.

As temperature is raised to the crystalline melting temperature of the nanofibers, T_m, the latent heat attributed to the thermodynamic transition leads to the observation of endothermic peak in the DSC curve. The endothermic peak location on the temperature axis is associated with the crystallite chemistry.

The plot of heat flow (mW) against temperature is achieved when the temperature increased from T_1 to T_2, and the shift in the enthalpy, ΔH, is correlated to the area under the curve, A:

$$\Delta H = kA \tag{13}$$

where k is an instrument constant.

This technique is widely used to study the degrees of molecular orientation for different electrospun polymer nanofibers such as PLLA [99], modified cellulose/poly (vinyl alcohol) (MC/PVA) [12], poly (benzimidazole) [49], polyamide 66 (PA66) [32], poly (lactic acid) (PLA), poly(ethylene oxide) (PEO), poly(ε-caprolactone) (PCL)

[69], and PAN [11]. The higher degrees of molecular orientation in the electrospun polymer nanofibers are achieved as compared to cast film of the polymers which are frequently confirmed. The crystallization temperatures of poly (ethylene terephthalate) (PET) and poly (ethylenenapthalate) (PEN) nanofibers were also investigated by using DSC [48].

The generation of polymer fibers from polymer solution generally changes the orientation of polymer chains. The configuration of the polymer chains within the nanofibers could be investigated by X-ray diffraction (XRD) technique beside DSC, which is described below.

Thermogravimetric Analysis (TGA)

Thermogravimetric analysis (TGA) provides useful information about material compositions through decomposing all organic contents at high temperatures with a uniform heating rate. In the TGA analysis, a plot of mass against temperature or time is generated to measure the changes in the chemical and physical features of materials. The obtained thermogravimetric curves provides useful data about the thermal stability of remained materials, polymerization, second-order phase transitions, solid/gas interactions, the expediencies of stabilizers and activators, dehydration, and pyrolysis. In this case, by increasing temperature at a consistent rate, the decrease in the mass or gain of a sample is recorded. In the TGA instruments, sample is placed in a balance with a platinum crucible which is located inside a programmable furnace. TGA procedure is generally performed under air gas, but other inert gases such as nitrogen could be used as well in the either first or second stage of test to prohibit oxidation and/or other undesired reactions. For instance, the amount of silica in the vinyl polymer–silica hybrids was measured by TGA which was in line with the stoichiometry analysis results. In another effort, the thermal stability of the neat and nanophased polypropylene was investigated by using TGA. The heat rate was set at 10 °C/min and the test was conducted under nitrogen gas. The initial decomposition was observed at 10% of the total weight loss which was started at 394 °C and 430 °C for neat and nanophased polypropylene, respectively. The decomposition temperatures for neat and nanophased polypropylene were 444 °C and 474 °C, respectively. It showed that the nanophased polypropylene is thermally more stable than the neat polypropylene.

Magnetic Characteristic Measurements

M-H Hysteresis Loop

Vibrating sample magnetometer (VSM) is used to characterize the magnetic behavior of the samples. The VSM traits on Faraday's law of induction indicates that the generation of electric field is attributed to varying in the magnetic field. The VSM performing principle is by first placing the sample to be evaluated in a constant magnetic field. This constant magnetic field is prone to magnetize the sample by lining up the magnetic domains or the individual magnetic spins, with the field if the sample is magnetic. Larger magnetization will be occurred if the constant field is

stronger. A magnetic field around the sample is created as a result of the magnetic dipole moment, which is well-known as magnetic stray field. As the sample is shifted up and down, the magnetic stray field is varying as a function of time, and it is sensing by a set of pick-up coils [34].

The hysteresis loops are obtained by using a VSM with different models, e.g., model 7400 series. An automatic measurement on the fundamental magnetization curve is provided by this equipment. Furthermore, it provides magnetic hysteresis graphs under static state of various magnetic materials, precise measurement on static magnetic behavior parameters such as coercivity (H_c), saturation magnetization (M_s), and remanence (Br). Magnetization in terms of applied field measurements is a time-dependent measurement of the magnetic moment of a sample as the magnetism is enhanced and declined in a hysteretic fashion.

A room temperature starting at zero applied fields is normally operated for the measurement of the hysteresis loop. First, the magnetic field is ramped to, e.g., 1 kOe in 100 Oe accresions, continued by ramping to 10 kOe in 1 kOe enhancements. The reversion magnetic field is applied at identical state of field spacings to −10 kOe. Eventually, the magnetic field is elevated to 12 kOe to carry out a complete measurement of the hysteresis loop. The M_s is identified by scrutinizing the magnetic moment of the sample at the largest applied magnetic field. H_c and M_r are estimated by placing the point on the x-axis and on the y-axis, respectively, where the magnetization is zero in an applied field:

$$M_S = 8.1661 \exp\left(\frac{3T}{1000}\right) \tag{14}$$

where T is temperature.

For example, the variation of H_c with particle size in $CoFe_2O_4$ nanofiber is shown in Fig. 6 [60]. It indicates that by increasing the calcination temperature, the particle size changes from single-domain to multi-domain state, determining the critical particle size for $CoFe_2O_4$ nanofiber. It also indicates the canted spin arrangement on the surface of particles, which is considered as "dead magnetic layer." This is associated with the thermal energy (KBT). When size reached nanoscale, thermal energy became more prominent and comparable to the magnetic anisotropy energy (K1V). This is described in terms of a core–shell scenario: a ferromagnetic (FM) core with a paramagnetic (PM) shell, as shown in Fig. 6, and the core is the source of the principal magnetic attributes. As the particles grow, their contribution to the PM shell relatively decreased. Such random surface spins have a significant influence on the magnetic moments. The larger grain sizes lead to a higher M_s. The variation of H_c with particle size, which raised from gradual increase in calcination temperature, is also stated elsewhere.

B-H Hysteresis Loop

B-H hysteresis loop is attained by performing, for example, a Linkjoin Technology MATS 2010 Static Hysteresisgraph. From the B-H curve, the parameters are the following: H_c, saturation induction (Bs), and flux density (Br). The measurement is

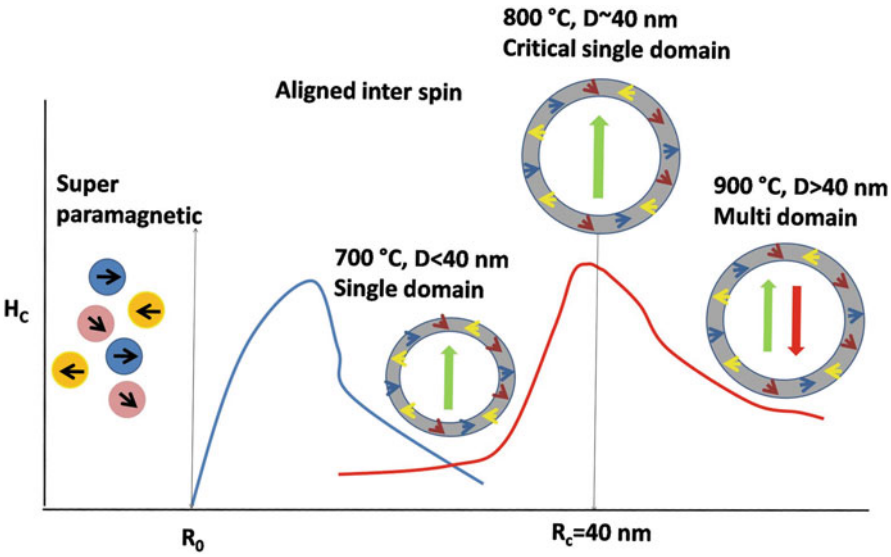

Fig. 6 Schematic illustration of H_c versus particle size (R) [60]

accomplished on the toroid samples at room temperature. Each sample is rounded with 60 turns for secondary turn (N2) with a copper wire and with 10 turns for primary turn (N1) with covered copper wire. Then, the samples connected to a B-H hysteresis graph and its curve are shown on the monitor [34].

Electrical and Dielectric Behavior Measurement

Dielectric Behaviors

The pellet form samples with thickness of 3 mm and diameter of 10 nm are used to measure the dielectric properties. The samples are placed between two sandwich-liked plates and then connected to instrument. The Novocontrol dielectric machine is used to measure dielectric properties such as dielectric constant and dielectric loss. It is interesting to mention that by using this machine there is no longer conversion of data and it directly gives the values of dielectric behaviors.

Electrical Resistivity Measurement and Evaluation

The issue with the resistance measurement is that it relies not only on the material out of which the wire is composed but also the wire geometry. For instance, the measured resistance would enhance by increasing the length or reducing the diameter of the used wire. However, to determine a behavior that explains a material's ability to carry electrical current that is independent of the geometrical factors, its resistivity is computed. In doing so, the electrical resistance (R) is measured by using, e.g., Keithley 6485 Picoammeter. To resistance measurement, the samples are

placed between parallel plates and attached to the instrument. A current is passed through the sample by conducting a metallic contact deposited at the end of each sample. In fact, after smoothly polishing the toroid-like samples by silica carbide paper, in order to make better electrical connection between the plates and sample, a silver paste is deposited on the samples. Then, the Eq. 15 is applied to compute the resistivity of the sample:

$$\rho = \frac{\mathrm{AR}}{t}\,\Omega\mathrm{cm} \tag{15}$$

where A and t refer to the cross-sectional area and thickness of the sample.

In composite nanofiber materials, in order to shift the composite from the insulative state into the conductive state, a critical filler loading (the percolation threshold) should be integrated. The electrical conductivity of the composite would suddenly enhance at the critical filler loading. As shown in Fig. 7, the filler generates an incessant network inside the polymer matrix at the percolation threshold. Enhancement in the filler loading results in a little effect on the composite electrical resistivity.

Once the filler loading increases above the percolation threshold, a remarkable reduction in the composite's electrical resistivity occurs [1]. In this state the three-dimensional conductive network does not form at the percolation concentration, and hence the composite conductivity is attributed to tunneling beside direct contact between the particles.

Tunneling conduction is the dominant mechanism in some cases. It occurs once the distance between the filler particles are small enough, approximately less than 10 nm. The current–voltage (I-V) relationship investigation indicates if the composite conductivity is because of tunneling or direct contact between the particles

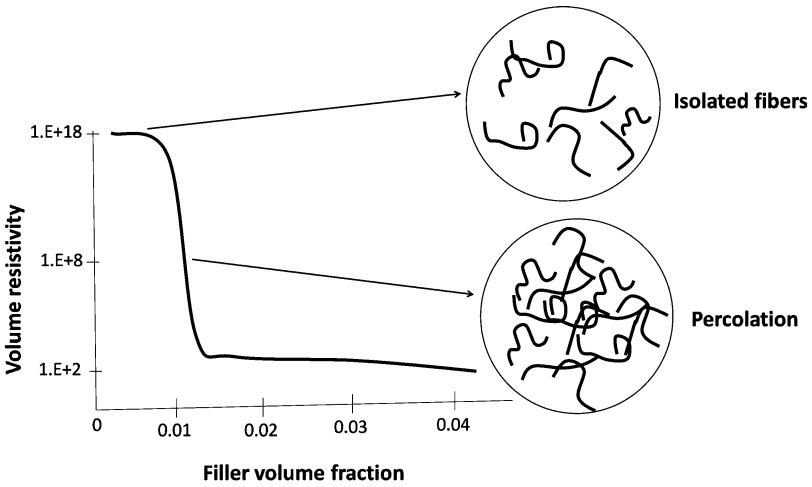

Fig. 7 Schematic of typical electrical resistivity as a function of filler loading of high aspect ratio filler/polymer system [1]

[96]. Linear I-V relationship (Ohm's law) shows that the dominant conduction mechanism is direct contact between the filler particles. Nevertheless, when composites are characterized by using power law I-V relation, the tunneling is the main mechanism [1, 13].

Characterization of Single Fiber

Due to the fact that nanofiber characterization is controlled by the properties of the individual fibers, characterization of single fibers is important for understanding physical, chemical, and mechanical properties of nanofibers. Assessment of single-fiber properties by interpreting of data obtained from the characterization of nanofibers samples is not practical. Nanofibers with dimensions smaller than the wavelength of light are complicated to extract or assess. Different novel approaches for the direct characterization of mechanical, electrical, optical, and thermal properties of single fibers are developed, and the mechanical properties of fibers are discussed in details in the following section [3, 50, 55]. Various conventional test techniques used in materials science have also been efficiently employed for nanofibers. For example, single electrospun nanofiber could practically be installed in a universal tensile test machine to monitor their properties [39, 87]. Besides, individual nanofibers of poly (L-lactide) (PLLA) and poly (1-caprolactone) (PCL) nanofibers electrospun were successfully isolated and installed in a tensile test machine [40, 86, 87]. The tensile test of PCL yielded a tensile modulus of 120 $\pm$ 30 MPa and an ultimate extensibility of 200 $\pm$ 100%. In addition, however, AFM is mostly used for profilometric and surface chemistry study of materials; it can be used for measuring tensile properties of nanofiber to avoid some of the drawbacks attributed to the nanofibers handling during test procedure. This technique has been also served as an appropriate system in monitoring mechanical properties of individual nanofibers [38]. For instance, tensile properties of single-walled carbon nanotubes (SWCNTs) and multi-walled carbon nanotubes (MWCNTs) have been measured through AFM study [17].

The AFM instruments can be used for nanoindentation measurement, bending test, and uniaxial extension test in the nanofibers. For nanoindentation measurements, the AFM is operated in the force mode when tip is in contact with the sample surface. To obtain more meaningful information, the small diameter tip is required and the data should be collected at the same strain rate. The indentation depth, dZ, diverges linearly with the utilized load, p. The slope of the curve at P_{max} is directly correlated to the Young's modulus, E^*, of the nanofibers, and A is the sample area where tip is connected:

$$\text{Slope} = \{\mathrm{dP}/\mathrm{dZ}\}_{\max} = 2E^*(A/\pi)^{1/2} \tag{16}$$

The AFM is used for bending test by applying a deflecting force into nanofibers to measure Young's modulus, E^*. The applied force, F, by the tip at the fiber leads to a tip deflection, ΔZ, which can be converted to the fiber deformation, δ. The applied force, F, is attributed to the deformation of the sample, δ, as given below [98]:

$$\delta = F\left(L^3/\alpha E^* I\right) \tag{17}$$

where I, L, and α are the moment of inertia, the suspended length of the fiber, and constant value, respectively.

The AFM instrument has been applied on PEO [5], poly (dicyclopentadiene) [4], inorganic Ti nanofibers, TiO_2-filled poly (vinylpyrrolidone) (PVP) [53], polyacrylonitrile (PAN) [31], and PVA nanofibers [82] to measurement bending properties.

Using AFM for illustration of a complete stress–strain curve for an individual nanofiber is a challenging procedure [87]. Uniaxial extension test was used for aligned PEO nanofibers by using a piezoresistive AFM cantilever, and the elastic modulus of PEO nanofibers was estimated to be about of 45 MPa. In this case, the deflection data are converted to the electrical resistance of the piezoresistive cantilever to test the uniaxial load. The uniaxial extension information was measured from an image recorded by a charge-coupled device (CCD) camera.

The Raman spectroscopy could be used as a powerful technique to calculate the molecular orientation and structure of individual nanofibers. This technique has been used in the characterization of single electrospun poly (ethylene terephthalate) nanofibers [75].

Conclusions and Perspectives

Nanofibers as a relatively new developed type of nanomaterials satisfy many of drawbacks faced with nanomaterial synthesis procedures including low chemical and biological flexibility, toxicity, cost, and need for large-scale fabrication platforms. Therefore, nanofibers could open up a new window for extensive scientific and industrial applications of organic-based nanotechnology. Principal challenges in the characterization of nanofiber including limitation in the manipulating small nanofibers, the lack of confirmed appropriate techniques, finding an appropriate observation mode, finding a suitable source for force transducers and actuators, and single nanofibers sample preparation make it a complicated procedure. Moreover, nanofibers could simply degrade under harsh reaction conditions; so, when degradable polymers are used as samples, particular care should be taken to protect nanofibers from quick destruction or degradation during characterization process. Therefore, characterization of nanofibers is far from being ideal, and more attempts have to be done to perfectly characterize this speculate material for using nanofibers in various applications and future devices.

References

1. Al-Saleh MH, Sundararaj U (2009) A review of vapor grown carbon nanofiber/polymer conductive composites. Carbon 47:2–22. https://doi.org/10.1016/j.carbon.2008.09.039
2. Arinstein A, Burman M, Gendelman O, Zussman E (2007) Effect of supramolecular structure on polymer nanofibre elasticity. Nat Nanotechnol 2:59–62. https://doi.org/10.1038/nnano.2006.172

3. Balzer F, Bordo VG, Simonsen AC, Rubahn H-G (2003) Isolated hexaphenyl nanofibers as optical waveguides. Appl Phys Lett 82:10–12. https://doi.org/10.1063/1.1533845
4. Bellan LM, Coates GW, Craighead HG (2006) Poly(dicyclopentadiene) submicron fibers produced by electrospinning. Macromol Rapid Commun 27:511–515. https://doi.org/10.1002/marc.200500823
5. Bellan LM, Kameoka J, Craighead HG (2005) Measurement of the Young's moduli of individual polyethylene oxide and glass nanofibres. Nanotechnology 16:1095–1099. https://doi.org/10.1088/0957-4484/16/8/017
6. Bhowmick S, Fowler A, Warner SB, Meressi T, Gibson P (2007) Transport in 3-D nanofab geometries. National Textile Center Annual Reports, NTC Project F06-MD04
7. Birdi KSS (2003) Scanning probe microscopes: applications in science and technology. CRC Press, Boca Raton
8. Bognitzki M, Czado W, Frese T, Schaper A, Hellwig M, Steinhart M, Greiner A, Wendorff JH (2001) Nanostructured fibers via electrospinning. Adv Mater 13:70–72. https://doi.org/10.1002/1521-4095(200101)13:1<70::AID-ADMA70>3.0.CO;2-H
9. Boland ED, Wnek GE, Simpson DG, Pawlowski KJ, Bowlin GL (2001) Tailoring tissue engineering scaffolds using electrostatic processing techniques: a study of poly(glycolic acid) electrospinning. J Macromol Sci A: Pure Appl Chem 38:1231–1243
10. Buell S, Van Vliet KJ, Rutledge GC (2009) Mechanical properties of glassy polyethylene nanofibers via molecular dynamics simulations. Macromolecules 42:4887–4895. https://doi.org/10.1021/ma900250y
11. Buer A, Ugbolue SC, Warner SB (2001) Electrospinning and properties of some nanofibers. Text Res J 71:323–328. https://doi.org/10.1177/004051750107100408
12. Chahal S, Hussain FSJ, Yusoff MBM (2013) Characterization of modified cellulose (MC)/poly (vinyl alcohol) electrospun nanofibers for bone tissue engineering. Proc Eng 53:683–688. https://doi.org/10.1016/j.proeng.2013.02.088
13. Chekanov Y, Ohnogi R, Asai S, Sumita M (1999) Electrical properties of epoxy resin filled with carbon fibers. J Mater Sci 34:5589–5592
14. Chen K, Shen Z, Luo J, Wang X, Sun R (2015) Quaternized chitosan/silver nanoparticles composite as a SERS substrate for detecting tricyclazole and Sudan I. Appl Surf Sci 351:466–473. https://doi.org/10.1016/j.apsusc.2015.05.149
15. Chipara DM, Macossay J, Ybarra AVR, Chipara AC, Eubanks TM, Chipara M (2013) Raman spectroscopy of polystyrene nanofibers – multiwalled carbon nanotubes composites. Appl Surf Sci 275:23–27. https://doi.org/10.1016/j.apsusc.2013.01.116
16. Cuenot S, Frétigny C, Demoustier-Champagne S, Nysten B (2004) Surface tension effect on the mechanical properties of nanomaterials measured by atomic force microscopy. Phys Rev B 69:165410. https://doi.org/10.1103/PhysRevB.69.165410
17. Demczyk B, Wang Y, Cumings J, Hetman M, Han W, Zettl A, Ritchie R (2002) Direct mechanical measurement of the tensile strength and elastic modulus of multiwalled carbon nanotubes. Mater Sci Eng A 334:173–178. https://doi.org/10.1016/S0921-5093(01)01807-X
18. Demir M, Yilgor I, Yilgor E, Erman B (2002) Electrospinning of polyurethane fibers. Polymer 43:3303–3309. https://doi.org/10.1016/S0032-3861(02)00136-2
19. Dersch R, Liu T, Schaper AK, Greiner A, Wendorff JH (2003) Electrospun nanofibers: internal structure and intrinsic orientation. J Polym Sci A Polym Chem 41:545–553. https://doi.org/10.1002/pola.10609
20. Ding B, Fujimoto K, Shiratori S (2005) Preparation and characterization of self-assembled polyelectrolyte multilayered films on electrospun nanofibers. Thin Solid Films 491:23–28. https://doi.org/10.1016/j.tsf.2005.02.009
21. Ding B, Kim J, Miyazaki Y, Shiratori S (2004) Electrospun nanofibrous membranes coated quartz crystal microbalance as gas sensor for NH3 detection. Sensors Actuators B Chem 101:373–380. https://doi.org/10.1016/j.snb.2004.04.008
22. Ding B, Kimura E, Sato T, Fujita S, Shiratori S (2004) Fabrication of blend biodegradable nanofibrous nonwoven mats via multi-jet electrospinning. Polymer 45:1895–1902. https://doi.org/10.1016/j.polymer.2004.01.026

23. Duan B, Yuan X, Zhu Y, Zhang Y, Li X, Zhang Y, Yao K (2006) A nanofibrous composite membrane of PLGA–chitosan/PVA prepared by electrospinning. Eur Polym J 42:2013–2022. https://doi.org/10.1016/j.eurpolymj.2006.04.021
24. Esnaashari SS, Rezaei S, Mirzaei E, Afshari H, Rezayat SM, Faridi-Majidi R (2014) Preparation and characterization of kefiran electrospun nanofibers. Int J Biol Macromol 70:50–56. https://doi.org/10.1016/j.ijbiomac.2014.06.014
25. Gao Y, Yang Z, Kuang Y, Ma M-L, Li J, Zhao F, Xu B (2010) Enzyme-instructed self-assembly of peptide derivatives to form nanofibers and hydrogels. Biopolymers 94:19–31. https://doi.org/10.1002/bip.21321
26. Gebeyehu MB, Chang Y-H, Abay AK, Chang S-Y, Lee J-Y, Wu C-M, Chiang T-C, Murakami R-I (2016) Fabrication and characterization of continuous silver nanofiber/polyvinylpyrrolidone (AgNF/PVP) core–shell nanofibers using the coaxial electrospinning process. RSC Adv 6:54162–54168. https://doi.org/10.1039/C6RA05869H
27. Goldman A (1999) Handbook of modern ferromagnetic materials. Springer Science & Business Media. The Springer International Series in Engineering and Computer Science, Series Volume 505, Springer US, Boston, MA, https://doi.org/10.1007/978-1-4615-4917-8
28. Greiner A, Wendorff JH, Yarin AL, Zussman E (2006) Biohybrid nanosystems with polymer nanofibers and nanotubes. Appl Microbiol Biotechnol 71:387–393. https://doi.org/10.1007/s00253-006-0356-z
29. Griffith AA (1921) The phenomena of rupture and flow in solids. Philos Trans R Soc Lond 221:163–198
30. Gu S-Y, Ren J (2005) Process optimization and empirical modeling for electrospun poly(D, L-lactide) fibers using response surface methodology. Macromol Mater Eng 290:1097–1105. https://doi.org/10.1002/mame.200500215
31. Gu S-Y, Wu Q-L, Ren J, Vancso GJ (2005) Mechanical properties of a single electrospun fiber and its structures. Macromol Rapid Commun 26:716–720. https://doi.org/10.1002/marc.200400667
32. Guerrini LM, Branciforti MC, Canova T, Suman Bretas RE (2009) Electrospinning and characterization of polyamide 66 nanofibers with different molecular weights. Mater Res 12:181–190
33. Hajalilou A, Hashim M, Ebrahimi-Kahrizsangi R, Mohamed Kamari H, Sarami N (2014) Synthesis and structural characterization of nano-sized nickel ferrite obtained by mechanochemical process. Ceram Int 40:5881–5887. https://doi.org/10.1016/j.ceramint.2013.11.032
34. Hajalilou A, Hashim M, Ebrahimi-Kahrizsangi R, Sarami N (2015) Influence of CaO and SiO2 co-doping on the magnetic, electrical properties and microstructure of a Ni–Zn ferrite. J Phys D Appl Phys 48:145001
35. Hajalilou A, Kamari HM, Shameli K (2017) Dielectric and electrical characteristics of mechanically synthesized Ni–Zn ferrite nanoparticles. J Alloys Compd 708:813–826. https://doi.org/10.1016/j.jallcom.2017.03.030
36. Hou H, Ge JJ, Zeng J, Li Q, Reneker DH, Greiner A, Cheng SZD (2005) Electrospun polyacrylonitrile nanofibers containing a high concentration of well-aligned multiwall carbon nanotubes. Chem Mater 17:967–973. https://doi.org/10.1021/cm0484955
37. Huang Z-M, Zhang Y-Z, Kotaki M, Ramakrishna S (2003) A review on polymer nanofibers by electrospinning and their applications in nanocomposites. Compos Sci Technol 63:2223–2253. https://doi.org/10.1016/S0266-3538(03)00178-7
38. Hugel T (2002) Single-molecule optomechanical cycle. Science 296:1103–1106. https://doi.org/10.1126/science.1069856
39. Inai R, Kotaki M, Ramakrishna S (2005) Deformation behavior of electrospun poly(L-lactide-co-ϵ-caprolactone) nonwoven membranes under uniaxial tensile loading. J Polym Sci B Polym Phys 43:3205–3212. https://doi.org/10.1002/polb.20457
40. Inai R, Kotaki M, Ramakrishna S (2005) Structure and properties of electrospun PLLA single nanofibres. Nanotechnology 16:208–213. https://doi.org/10.1088/0957-4484/16/2/005

41. Jalili R, Morshed M, Ravandi SAH (2006) Fundamental parameters affecting electrospinning of PAN nanofibers as uniaxially aligned fibers. J Appl Polym Sci 101:4350–4357. https://doi.org/10.1002/app.24290
42. Jena AK, Gupta KM (1999) In-plane compression porometry of battery separators. J Power Sources 80:46–52. https://doi.org/10.1016/S0378-7753(99)00163-9
43. Ji Y, Li B, Ge S, Sokolov JC, Rafailovich MH (2006) Structure and nanomechanical characterization of electrospun PS/clay nanocomposite fibers. Langmuir 22:1321–1328. https://doi.org/10.1021/la0525022
44. Jia Y, Huang G, Dong F, Liu Q, Nie W (2016) Preparation and characterization of electrospun poly(ε-caprolactone)/poly(vinyl pyrrolidone) nanofiber composites containing silver particles. Polym Compos 37:2847–2854. https://doi.org/10.1002/pc.23481
45. Karageorgiou V, Kaplan D (2005) Porosity of 3D biomaterial scaffolds and osteogenesis. Biomaterials 26:5474–5491. https://doi.org/10.1016/j.biomaterials.2005.02.002
46. Kim C, Park S-H, Cho J-I, Lee D-Y, Park T-J, Lee W-J, Yang K-S (2004) Raman spectroscopic evaluation of polyacrylonitrile-based carbon nanofibers prepared by electrospinning. J Raman Spectrosc 35:928–933. https://doi.org/10.1002/jrs.1233
47. Kim HS, Jin H-J, Myung SJ, Kang M, Chin I-J (2006) Carbon nanotube-adsorbed electrospun nanofibrous membranes of nylon 6. Macromol Rapid Commun 27:146–151. https://doi.org/10.1002/marc.200500617
48. Kim J-S, Lee DS (2000) Thermal properties of electrospun polyesters. Polym J 32:616–618. https://doi.org/10.1295/polymj.32.616
49. Kim J-S, Reneker DH (1999) Polybenzimidazole nanofiber produced by electrospinning. Polym Eng Sci 39:849–854. https://doi.org/10.1002/pen.11473
50. Kitazawa M, Ohta R, Tanaka J, Tanemura M (2007) Electrical properties of single carbon nanofibers grown on tips of scanning probe microscope cantilevers by ion irradiation. Jpn J Appl Phys 46:5607–5610. https://doi.org/10.1143/JJAP.46.5607
51. Ko F, Gogotsi Y, Ali A, Naguib N, Ye H, Yang GL, Li C, Willis P (2003) Electrospinning of continuous carbon nanotube-filled nanofiber yarns. Adv Mater 15:1161–1165. https://doi.org/10.1002/adma.200304955
52. Lee IW, Li J, Chen X, Park HJ (2016) Electrospun poly(vinyl alcohol) composite nanofibers with halloysite nanotubes for the sustained release of sodium D-pantothenate. J Appl Polym Sci 133. doi:https://doi.org/10.1002/app.42900
53. Lee S-H, Tekmen C, Sigmund WM (2005) Three-point bending of electrospun TiO2 nanofibers. Mater Sci Eng A 398:77–81. https://doi.org/10.1016/j.msea.2005.03.014
54. Li M, Mondrinos MJ, Gandhi MR, Ko FK, Weiss AS, Lelkes PI (2005) Electrospun protein fibers as matrices for tissue engineering. Biomaterials 26:5999–6008. https://doi.org/10.1016/j.biomaterials.2005.03.030
55. Li Q, Liu C, Wang X, Fan S (2009) Measuring the thermal conductivity of individual carbon nanotubes by the Raman shift method. Nanotechnology 20:145702. https://doi.org/10.1088/0957-4484/20/14/145702
56. Li W-J, Laurencin CT, Caterson EJ, Tuan RS, Ko FK (2002) Electrospun nanofibrous structure: a novel scaffold for tissue engineering. J Biomed Mater Res 60:613–621. https://doi.org/10.1002/jbm.10167
57. Lin S, Cai Q, Ji J, Sui G, Yu Y, Yang X, Ma Q, Wei Y, Deng X (2008) Electrospun nanofiber reinforced and toughened composites through in situ nano-interface formation. Compos Sci Technol 68:3322–3329. https://doi.org/10.1016/j.compscitech.2008.08.033
58. Liu W, Wu Z, Reneker DH (2000) Structure and morphology of poly(metaphenylene isophthalamide) nanofibers produced by electrospinning. Polym Prepr 41:1193–1194
59. Liu Y, Cui L, Guan F, Gao Y, Hedin NE, Zhu L, Fong H (2007) Crystalline morphology and polymorphic phase transitions in electrospun nylon-6 nanofibers. Macromolecules 40:6283–6290. https://doi.org/10.1021/ma070039p
60. Lu R, Chang K, Fu B, Shen Y, Xu M, Yang S, Song X, Liu M (2014) Magnetic properties of different CoFe2O4 nanostructures: nanofibers versus nanoparticles. J Mater Chem C 2:8578–8584

61. Luu YK, Kim K, Hsiao BS, Chu B, Hadjiargyrou M (2003) Development of a nanostructured DNA delivery scaffold via electrospinning of PLGA and PLA–PEG block copolymers. J Control Release 89:341–353. https://doi.org/10.1016/S0168-3659(03)00097-X
62. Ma Z, Kotaki M, Inai R, Ramakrishna S (2005) Potential of nanofiber matrix as tissue-engineering scaffolds. Tissue Eng 11:101–109. https://doi.org/10.1089/ten.2005.11.101
63. Marcos M, Cano P, Fantazzini P, Garavaglia C, Gomez S, Garrido L (2006) NMR relaxometry and imaging of water absorbed in biodegradable polymer scaffolds. Magn Reson Imaging 24:89–95. https://doi.org/10.1016/j.mri.2005.10.008
64. Mathew G, Hong JP, Rhee JM, Lee HS, Nah C (2005) Preparation and characterization of properties of electrospun poly(butylene terephthalate) nanofibers filled with carbon nanotubes. Polym Test 24:712–717. https://doi.org/10.1016/j.polymertesting.2005.05.002
65. McKee MG, Park T, Unal S, Yilgor I, Long TE (2005) Electrospinning of linear and highly branched segmented poly(urethane urea)s. Polymer 46:2011–2015. https://doi.org/10.1016/j.polymer.2005.01.028
66. McManus MC, Boland ED, Koo HP, Barnes CP, Pawlowski KJ, Wnek GE, Simpson DG, Bowlin GL (2006) Mechanical properties of electrospun fibrinogen structures. Acta Biomater 2:19–28. https://doi.org/10.1016/j.actbio.2005.09.008
67. Miller RE, Shenoy VB (2000) Size-dependent elastic properties of nanosized structural elements. Nanotechnology 11:139–147. https://doi.org/10.1088/0957-4484/11/3/301
68. Morozov V, Morozova T, Kallenbach N (1998) Atomic force microscopy of structures produced by electrospraying polymer solutions. Int J Mass Spectrom 178:143–159. https://doi.org/10.1016/S1387-3806(98)14083-6
69. Oliveira JE, Mattoso LHC, Orts WJ, Medeiros ES (2013) Structural and morphological characterization of micro and nanofibers produced by electrospinning and solution blow spinning: a comparative study. Adv Mater Sci Eng 1–14. doi:https://doi.org/10.1155/2013/409572
70. Paiva-Santos CO, Gouveia H, Las WC, Varela JA (1999) Gauss-Lorentz size-strain broadening and cell parameters analysis of Mn doped SnO2 prepared by organic route. Mater Struct 6:111–115
71. Patel AC, Li S, Yuan J-M, Wei Y (2006) In situ encapsulation of horseradish peroxidase in electrospun porous silica fibers for potential biosensor applications. Nano Lett 6:1042–1046. https://doi.org/10.1021/nl0604560
72. Pedicini A, Farris RJ (2003) Mechanical behavior of electrospun polyurethane. Polymer 44:6857–6862. https://doi.org/10.1016/j.polymer.2003.08.040
73. Pirlot C, Mekhalif Z, Fonseca A, Nagy JB, Demortier G, Delhalle J (2003) Surface modifications of carbon nanotube/polyacrylonitrile composite films by proton beams. Chem Phys Lett 372:595–602. https://doi.org/10.1016/S0009-2614(03)00464-0
74. Ren S, Dong L, Zhang X, Lei T, Ehrenhauser F, Song K, Li M, Sun X, Wu Q (2017) Electrospun nanofibers made of silver nanoparticles, cellulose nanocrystals, and polyacrylonitrile as substrates for surface-enhanced Raman scattering. Materials 10:68. https://doi.org/10.3390/ma10010068
75. Richard-Lacroix M, Pellerin C (2012) Orientation and structure of single electrospun nanofibers of poly(ethylene terephthalate) by confocal Raman spectroscopy. Macromolecules 45:1946–1953. https://doi.org/10.1021/ma202749d
76. Roodbar Shojaei T, Mohd Salleh MA, Sijam K, Abdul Rahim R, Mohsenifar A, Safarnejad R, Tabatabaei M (2016) Fluorometric immunoassay for detecting the plant virus citrus tristeza using carbon nanoparticles acting as quenchers and antibodies labeled with CdTe quantum dots. Microchim Acta 183:2277–2287. https://doi.org/10.1007/s00604-016-1867-7
77. Roodbar Shojaei T, Mohd Salleh MA, Sijam K, Abdul Rahim R, Mohsenifar A, Safarnejad R, Tabatabaei M (2016) Detection of citrus tristeza virus by using fluorescence resonance energy transfer-based biosensor. Spectrochim Acta A Mol Biomol Spectrosc 169:216–222. https://doi.org/10.1016/j.saa.2016.06.052

78. Roodbar Shojaei T, Mohd Salleh MA, Tabatabaei M, Ekrami A, Motallebi R, Rahmani-Cherati T, Hajalilou A, Jorfi R (2014) Development of sandwich-form biosensor to detect mycobacterium tuberculosis complex in clinical sputum specimens. Braz J Infect Dis 18:600–608. https://doi.org/10.1016/j.bjid.2014.05.015
79. Sasipriya K, Suriyaprabha R, Prabu P, Rajendran V (2013) Synthesis and characterisation of polymeric nanofibers poly (vinyl alcohol) and poly (vinyl alcohol)/silica using indigenous electrospinning set up. Mater Res 16:824–830. https://doi.org/10.1590/S1516-14392013005000050
80. Schreuder-Gibson H, Gibson P (2006) Applications of electrospun nanofibers in current and future materials. In: Reneker DH, Fong H (eds) Polymer nanofibers. ACS Symposium Series, Vol. 918, American Chemical Society Publication, Washington D.C, USA, page 121–136 https://doi.org/10.1021/bk-2006-0918.ch009
81. Seah MP (1999) Quantitative AES and XPS: convergence between theory and experimental databases. J Electron Spectrosc Relat Phenom 100:55–73. https://doi.org/10.1016/S0368-2048(99)00040-7
82. Shin MK, Kim SI, Kim SJ, Kim S-K, Lee H (2006) Reinforcement of polymeric nanofibers by ferritin nanoparticles. Appl Phys Lett 88:193901. https://doi.org/10.1063/1.2200469
83. Silva GA (2004) Selective differentiation of neural progenitor cells by high-epitope density nanofibers. Science 303:1352–1355. https://doi.org/10.1126/science.1093783
84. Srinivasan G, Reneker DH (1995) Structure and morphology of small diameter electrospun aramid fibers. Polym Int 36:195–201. https://doi.org/10.1002/pi.1995.210360210
85. Sun Y, Yin Y, Mayers BT, Herricks T, Xia Y (2002) Uniform silver nanowires synthesis by reducing AgNO3 with ethylene glycol in the presence of seeds and poly(vinyl pyrrolidone). Chem Mater 14:4736–4745. https://doi.org/10.1021/cm020587b
86. Tan EPS, Lim CT (2006) Mechanical characterization of nanofibers – a review. Compos Sci Technol 66:1102–1111. https://doi.org/10.1016/j.compscitech.2005.10.003
87. Tan EPS, Ng SY, Lim CT (2005) Tensile testing of a single ultrafine polymeric fiber. Biomaterials 26:1453–1456. https://doi.org/10.1016/j.biomaterials.2004.05.021
88. Thandavamoorthy S, Gopinath N, Ramkumar SS (2006) Self-assembled honeycomb polyurethane nanofibers. J Appl Polym Sci 101:3121–3124. https://doi.org/10.1002/app.24333
89. Tian M, Gao Y, Liu Y, Liao Y, Xu R, Hedin NE, Fong H (2007) Bis-GMA/TEGDMA dental composites reinforced with electrospun nylon 6 nanocomposite nanofibers containing highly aligned fibrillar silicate single crystals. Polymer 48:2720–2728. https://doi.org/10.1016/j.polymer.2007.03.032
90. Tomlins P (2004) Characterisation and design of tissue scaffolds. Woodhead Publishing, Oxford, UK
91. Torrisi A (2008) XPS study of five fluorinated compounds deposited on calcarenite stone. Appl Surf Sci 254:2650–2658. https://doi.org/10.1016/j.apsusc.2007.10.003
92. Wang X, Chen X, Yoon K, Fang D, Hsiao BS, Chu B (2005) High flux filtration medium based on nanofibrous substrate with hydrophilic nanocomposite coating. Environ Sci Technol 39:7684–7691. https://doi.org/10.1021/es050512j
93. Xu LR, Li L, Lukehart CM, Kuai H (2007) Mechanical characterization of nanofiber-reinforced composite adhesives. J Nanosci Nanotechnol 7:2546–2548
94. Yang F, Xu CY, Kotaki M, Wang S, Ramakrishna S (2004) Characterization of neural stem cells on electrospun poly(L-lactic acid) nanofibrous scaffold. J Biomater Sci Polym Ed 15:1483–1497. https://doi.org/10.1163/1568562042459733
95. Yang T, Yang H, Zhen SJ, Huang CZ (2015) Hydrogen-bond-mediated in situ fabrication of AgNPs/Agar/PAN electrospun nanofibers as reproducible SERS substrates. ACS Appl Mater Interfaces 7:1586–1594. https://doi.org/10.1021/am507010q
96. Yui H, Wu G, Sano H, Sumita M, Kino K (2006) Morphology and electrical conductivity of injection-molded polypropylene/carbon black composites with addition of high-density polyethylene. Polymer 47:3599–3608. https://doi.org/10.1016/j.polymer.2006.03.064

97. Zhong WH, Li J, Xu LR, Michel JA, Sullivan LM, Lukehart CM (2004) Graphitic carbon nanofiber (GCNF)/polymer materials. I. GCNF/epoxy monoliths using hexanediamine linker molecules. J Nanosci Nanotechnol 4:794–802
98. Zhou W, Wu Y, Wei F, Luo G, Qian W (2005) Elastic deformation of multiwalled carbon nanotubes in electrospun MWCNTs–PEO and MWCNTs–PVA nanofibers. Polymer 46:12689–12695. https://doi.org/10.1016/j.polymer.2005.10.114
99. Zong X, Kim K, Fang D, Ran S, Hsiao BS, Chu B (2002) Structure and process relationship of electrospun bioabsorbable nanofiber membranes. Polymer 43:4403–4412. https://doi.org/10.1016/S0032-3861(02)00275-6
100. Zong X, Ran S, Fang D, Hsiao BS, Chu B (2003) Control of structure, morphology and property in electrospun poly(glycolide-co-lactide) non-woven membranes via post-draw treatments. Polymer 44:4959–4967. https://doi.org/10.1016/S0032-3861(03)00464-6
101. Zong X, Ran S, Kim K-S, Fang D, Hsiao BS, Chu B (2003) Structure and morphology changes during in vitro degradation of electrospun poly(glycolide- co -lactide) nanofiber membrane. Biomacromolecules 4:416–423. https://doi.org/10.1021/bm025717o
102. Zussman E, Chen X, Ding W, Calabri L, Dikin DA, Quintana JP, Ruoff RS (2005) Mechanical and structural characterization of electrospun PAN-derived carbon nanofibers. Carbon 43:2175–2185. https://doi.org/10.1016/j.carbon.2005.03.031